STRUCTURAL BIOLOGY COMMUNICATIONS

ISSN 2053-230X

Received 30 December 2016
Accepted 13 March 2017

Edited by W. N. Hunter, University of Dundee, Scotland

Keywords: enolase; crystal structure; active site; dimerization; glycolysis; *Drosophila melanogaster*.

PDB reference: *D. melanogaster* enolase, 5wro

Supporting information: this article has supporting information at journals.iucr.org/f

Crystal structure of enolase from *Drosophila melanogaster*

Congcong Sun,[a] Baokui Xu,[b] Xueyan Liu,[a] Zhen Zhang[c]* and Zhongliang Su[a]*

[a]College of Chemical Engineering, Qingdao University of Science and Technology, Qingdao, Shandong 266042, People's Republic of China, [b]Jianghuai College, Anhui University, Hefei, Anhui 230039, People's Republic of China, and [c]Laboratory for TCM Immunopharmacology and Molecular Biology, Institute of Basic Medicine, Shandong Academy of Medical Sciences, 18877 Jingshi Road, Jinan, Shandong 250062, People's Republic of China. *Correspondence e-mail: wwzhangzhen@126.com, albertszhl@126.com

Enolase is an important enzyme in glycolysis and various biological processes. Its dysfunction is closely associated with diseases. Here, the enolase from *Drosophila melanogaster* (DmENO) was purified and crystallized. A crystal of DmENO diffracted to 2.0 Å resolution and belonged to space group *R*32. The structure was solved by molecular replacement. Like most enolases, DmENO forms a homodimer with conserved residues in the dimer interface. DmENO possesses an open conformation in this structure and contains conserved elements for catalytic activity. This work provides a structural basis for further functional and evolutionary studies of enolase.

1. Introduction

Enolase (EC 4.2.1.11), also known as 2-phospho-D-glycerate hydrolase, belongs to the enolase superfamily, which contains the mandelate racemase (MR) and muconate-lactonizing (MLE) families (Gerlt *et al.*, 2005). Enolase is involved in the glycolytic pathway. It catalyzes the dehydration of 2-phospho-D-glycerate (PGA) to phosphoenolpyruvate (PEP) in catabolic metabolism and the reverse reaction during gluconeogenesis. Besides its role in metabolism, enolase also functions in other physiological processes. In vertebrates, enolase has three isozymes: enolase α (ENO1), β (ENO3) and γ (ENO2). In humans, ENO1 (HsENO1) is ubiquitously expressed, while HsENO2 is specifically expressed in muscle and HsENO3 in neurons (Isgrò *et al.*, 2015). Although the three isozymes have highly conserved sequences (about 83% identity; Supplementary Fig. S1), they possess specific functions (Pancholi, 2001; Díaz-Ramos *et al.*, 2012; Isgrò *et al.*, 2015). For example, HsENO1 can locate at the cell surface, where it functions as a plasminogen receptor to regulate pericellular fibrinolytic activity, as well as in the nucleus, where it binds to the c-Myc promoter region to regulate gene transcription (López-Alemany *et al.*, 2003; Feo *et al.*, 2000; Subramanian & Miller, 2000). Enolases are also involved in many pathological conditions. The upregulation of HsENO1 is associated with tumour progression, autoimmune diseases and neurological disorders (Díaz-Ramos *et al.*, 2012). HsENO3 is considered as a biomarker for many tumours, such as those found in the neuroendocrine system and in lung cancer (Isgrò *et al.*, 2015).

Enolase is an evolutionarily conserved enzyme and is widely present in prokaryotic and eukaryotic cells. There are two enolases, enolase 1 (ScENO1) and 2 (ScENO2), in *Saccharomyces cerevisiae* and one enolase in *Escherichia coli* (EcENO), which show 52–63% identity to human enolases

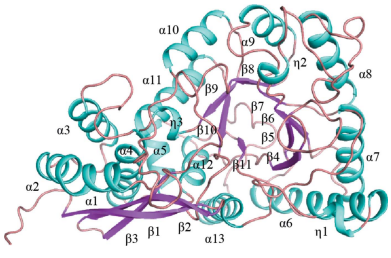

(Supplementary Fig. S1). These enolases have similar structural folds and conserved residues for catalysis (Reed *et al.*, 1996). They have been shown to occur as a homodimer in known structures (Stec & Lebioda, 1990; Kühnel & Luisi, 2001; Chai *et al.*, 2004). However, some enolase proteins from species such as *Bacillus subtilis*, *Staphylococcus aureus*, *Streptococcus pneumoniae* and *Streptococcus suis* have been found to be octamers (Ehinger *et al.*, 2004; Lu *et al.*, 2012; Newman *et al.*, 2012; Wu *et al.*, 2015). In these cases, an octameric conformation was found to be required for their catalytic activities.

Enolase possesses a bi-domain architecture with an N-terminal capping domain and a C-terminal β/α-barrel domain (Reed *et al.*, 1996; Pancholi, 2001; Díaz-Ramos *et al.*, 2012). The active site of enolase is located at the interface between the capping domain and the β/α-barrel domain. The catalytic reaction requires a divalent metal ion such as a magnesium ion, which is a natural cofactor of enolase. The two magnesium ions in the active site orchestrate the substrate and the conserved residues for catalysis.

Drosophila melanogaster is a good model organism for genetic and developmental studies. It has one enolase gene that encodes two proteins: the longer isoform 1 and the shorter isoform 2 (UniProt accession code P15007). Compared with isoform 2, *D. melanogaster* enolase (DmENO) isoform 1 has an extra N-terminal region that is not present in other enolases (Supplementary Fig. S1). This extra N-terminal part was predicted to be folded as a coil with a partially disordered region by the *PSIPRED* server (http://bioinf.cs.ucl.ac.uk/psipred/; Buchan *et al.*, 2013). Although DmENO and HsENO are highly conserved (73% sequence identity; Supplementary Fig. S1), it has been shown that these two enolases participate in variable interaction networks by bioinformatics analysis (Paludo *et al.*, 2015). In this study, we purified and crystallized recombinant DmENO isoform 2. The crystal structure was solved by molecular replacement. In this structure, DmENO forms a homodimer in an open conformation and has a similar overall structure to those of other enolases.

2. Materials and methods

2.1. Cloning and protein expression

The DNA sequence encoding DmENO isoform 2 corresponding to amino acids 68–500 of the longer isoform 1 was amplified from the cDNA of S2 cells and digested with the restriction enzymes EcoRI and XhoI. The forward and reverse primers are 5′-CCGGAATTCATGACCATCAAAGCGATC-3′ and 5′-CCGCTCGAGTTACTGCGGCTTCCTGAAC-3′ (the underlined nucleotides are the recognition sites for the restriction enzymes). The product was ligated into a modified pET-28a vector with an N-terminal 6×His tag and a TEV (*Tobacco etch virus*) protease site. The plasmid for expression was transformed into *E. coli* BL21 (DE3) CodonPlus competent cells. The cells were incubated in Terrific Broth medium with 30 μg ml^{-1} kanamycin and 34 μg ml^{-1} chloramphenicol at 37°C and protein expression was induced with 0.5 m*M* isopropyl β-D-1-thiogalactopyranoside at 20°C for 16 h.

2.2. Protein purification

Protein purification was performed at 4°C. The *E. coli* cells were collected at about 6400*g* for 10 min and suspended in five times the volume of lysis buffer consisting of 20 m*M* HEPES–Na pH 7.5, 500 m*M* NaCl, 5% glycerol, 20 m*M* imidazole, 1 m*M* DTT, 1 m*M* phenylmethylsulfonyl fluoride and then broken using a high-pressure homogenizer (JNBIO JN-3000 PLUS) at 130 MPa. Cell debris was removed by centrifugation for 40 min at 31 000*g*. The supernatant was mixed with pre-equilibrated Ni^{2+} Sepharose (GE Healthcare) for 1 h and the beads were then sequentially washed with lysis buffer containing 20 and 40 m*M* imidazole. The protein was eluted with lysis buffer plus 300 m*M* imidazole. The protein was concentrated using a 10 kDa cutoff Amicon Ultra-15 (Millipore) and exchanged into 20 m*M* HEPES–Na pH 7.5, 250 m*M* NaCl, 5% glycerol using a HiTrap Desalting column (GE Healthcare). The protein was then treated with His-tagged TEV protease and reapplied onto an Ni^{2+} Sepharose column to remove the protease and cleaved tag. Finally, the product was concentrated and loaded onto a HiLoad 16/60 Superdex 200 pg column (GE Healthcare) using 20 m*M* HEPES–Na pH 7.5, 100 m*M* NaCl, 1 m*M* DTT as the running buffer. The protein was concentrated to 10 mg ml^{-1}, with the concentration being determined by the Bradford method (Bio-Rad Protein Assay).

2.3. Crystallization and data collection

Crystallization experiments were performed by the sitting-drop vapour-diffusion method at 16°C. Crystallization kits from Hampton Research and Molecular Dimensions were used for crystallization screening. The 2 μl sitting drops consisted of 1 μl protein solution and 1 μl reservoir solution and were equilibrated against 100 μl reservoir solution. Crystals were optimized using the sitting-drop and hanging-drop vapour-diffusion methods.

Crystals were soaked in reservoir solution containing 20% glycerol and flash-cooled in liquid nitrogen. Diffraction data were collected from a single DmENO crystal on beamline BL17U at Shanghai Synchrotron Radiation Facility (SSRF), People's Republic of China with a Rayonix MX-225 CCD detector using 1° oscillations. The crystal-to-detector distance was 300 mm. A total of 180 diffraction frames were collected. Diffraction data were processed using *HKL*-2000 (Otwinowski & Minor, 1997) and *iMosflm* (Battye *et al.*, 2011) from the *CCP*4 software suite (Winn *et al.*, 2011). The initial space group was suggested to be *C*2 with an element of twinning, while the correct space group was *R*32 when the primary data were reprocessed after review.

2.4. Structure determination and refinement

The structure of DmENO was solved by molecular replacement with *Phaser* (McCoy *et al.*, 2007) using the HsENO1 structure (PDB entry 3b97; Kang *et al.*, 2008) as a

Table 1
Data-collection and refinement statistics for DmENO.

Values in parentheses are for the highest resolution shell.

Data collection	
Wavelength (Å)	0.97915
Space group	*R*32
Unit-cell parameters (Å, °)	$a = b = 118.82$, $c = 229.79$, $\alpha = \beta = 90$, $\gamma = 90$
Resolution (Å)	93.9–2.02 (2.07–2.02)
Total No. of reflections	367938 (23567)
No. of unique reflections	41492 (3019)
R_{merge}	0.189 (0.841)
$\langle I/\sigma(I)\rangle$	7.3 (2.2)
Completeness (%)	100.0 (100.0)
Multiplicity	8.9 (7.8)
Wilson *B* factor (Å^2)	29.0
Refinement	
Resolution (Å)	38.33–2.02 (2.09–2.02)
R_{work}	0.162
R_{free}	0.201
No. of atoms	
Total	3673
Protein	3308
Ligand/ion	32
Water	333
R.m.s.d.s	
Bond lengths (Å)	0.017
Bond angles (°)	0.830
Ramachandran plot	
Favoured (%)	97.25
Allowed (%)	2.29
Outliers (%)	0.46
Average *B* factors (Å^2)	
Overall	40.99
Protein	40.16
Ligand/ion	55.40
Water	47.82

search model. The model was completed using iterative cycles of manual building in *Coot* (Emsley *et al.*, 2010) and refinement with *phenix.refine* in *PHENIX* (Afonine *et al.*, 2012; Adams *et al.*, 2010) and *REFMAC*5 in *CCP*4 (Murshudov *et al.*, 2011; Winn *et al.*, 2011). The translation–libration–screw (TLS) method was used during structural refinement. The assignment of metal and chloride ions was based on difference density peak heights and the chemical environment. Structural images were produced in *PyMOL* (http://www.pymol.org/).

2.5. Structure deposition

The coordinates and structure factors for the crystal structure of DmENO were deposited in the Worldwide Protein Data Bank (wwPDB) under the accession code 5wro.

3. Results and discussion

3.1. Determination of the structure of DmENO

DmENO isoform 2 was purified by affinity chromatography and gel filtration (Supplementary Fig. S2*a*). There were two major peaks in the gel filtration. Nearly all of the DmENO sample was present in the second peak, which was used for crystal screening. Small crystals appeared in one week using a solution consisting of 10 m*M* $CoCl_2$, 0.1 *M* MES pH 6.5, 1.9 *M* ammonium sulfate. After systematical optimization including additive screening, trigonal crystals grew in 10 m*M* $CoCl_2$, 0.1 *M* MES pH 6.5, 1.9 *M* ammonium sulfate, 0.1 *M* $CdCl_2$ (Supplementary Fig. S2*b*). One of these crystals diffracted to 2.02 Å resolution and belonged to space group *R*32 (Table 1). The multiplicity and completeness of the data set were 8.9 and 100%, respectively. The structure was determined by molecular replacement using the structure of HsENO1 (PDB entry 3b97; Kang *et al.*, 2008) as a search model. The model was refined to a final R_{work} of 0.162 and R_{free} of 0.201. Details of the data-collection and refinement statistics are summarized in Table 1.

3.2. Crystal structure of DmENO

Only one molecule of DmENO is present in the asymmetric unit. DmENO contains 11 β-strands, 13 α-helices and three short 3_{10}-helices (notated as η-helices), and can be divided into two domains, like enolases from other species (Fig. 1). The N-terminal capping domain is composed of the first three β-strands and five α-helices, and the remaining part is the C-terminal β/α-barrel domain.

DmENO forms a butterfly-like homodimer with one symmetry-related molecule (Fig. 2*a*). The area of the interface for the DmENO homodimer is 1840 Å^2 (*PDBePISA* server; http://www.ebi.ac.uk/msd-srv/prot_int/pistart.html). Dimerization is mainly mediated by the β1 and β2 strands, the α6, α13 and η1 helices, the β1/β2 turn and the β3/α1, β4/α5, η1/α7 and β10/α12 loops (Fig. 2*b*). Arg76 in the β1 strand, Glu88 in the β2 strand, Glu445 in the β10/α12 loop and Asn123 in the β3/α1 loop of one chain form three ionic bonds and four hydrogen bonds to Lys250 in the α6 helix and Asn476, Arg480 and Glu483 in the α13 helix of the other chain *via* their side chains (Figs. 2*b* and 2*c*). The side chains of Ser253, Glu254 and His257 in the α6 helix, Asp270 in the η1 helix and Glu470 and Asn476 in the α13 helix from one chain contact the main chains of Tyr79 in the β1 strand, Arg82 and Gly83 in the β1/β2 turn, Tyr124 in the β3/α1 loop, Gly227 in the β4/α5 loop and Ser469 in the α13 helix from the other chain *via* hydrogen

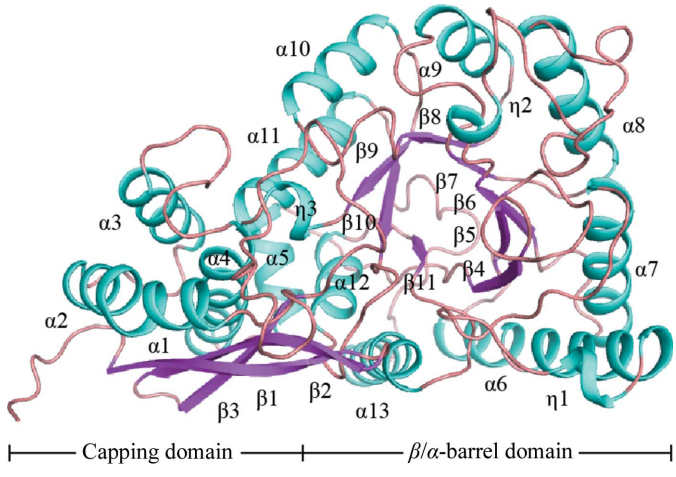

Figure 1
The overall structure of DmENO shown as a cartoon representation, with α-helices and η-helices coloured cyan and β-strands coloured pink. Each secondary-structure element is labelled according to its position in the amino-acid sequence.

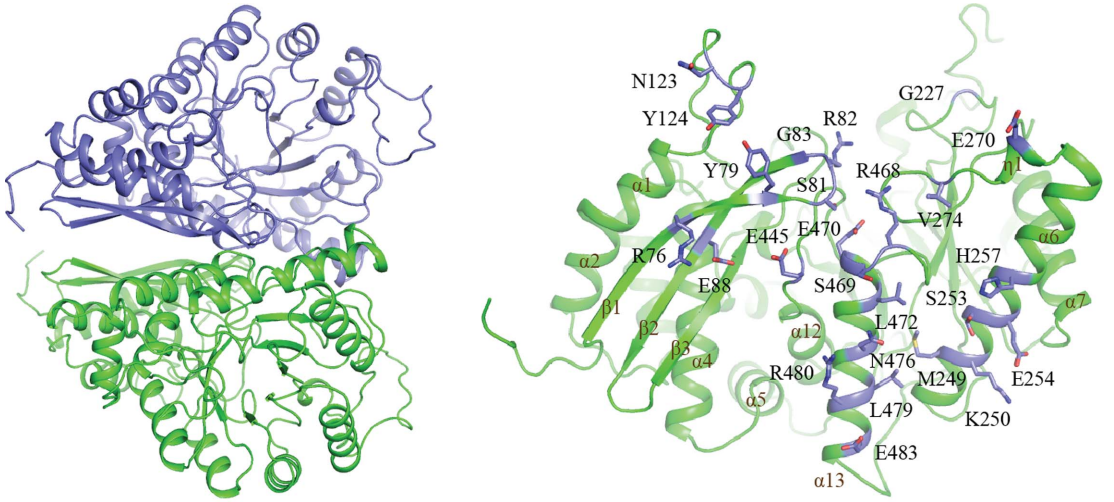

(*a*) (*b*)

Hydrogen bonds/salt bridges

Residue 1	Residue 2
R76	E483
Y79	S253
Y79	N476
S81	R468
R82	H257
E88	R480
N123	K250
Y124	E254
G227	D270
V274	V274
E445	N476
E445	R480
S469	E470

(*c*)

Figure 2
(*a*) DmENO forms a homodimer. The two DmENO chains are coloured green and slate. (*b*) Dimeric interface of DmENO. Residues at the interface are coloured slate and shown as sticks. (*c*) A list of the residues at the dimeric interface involved in the formation of hydrogen bonds and salt bridges. Residues forming both hydrogen bonds and salt bridges are coloured red.

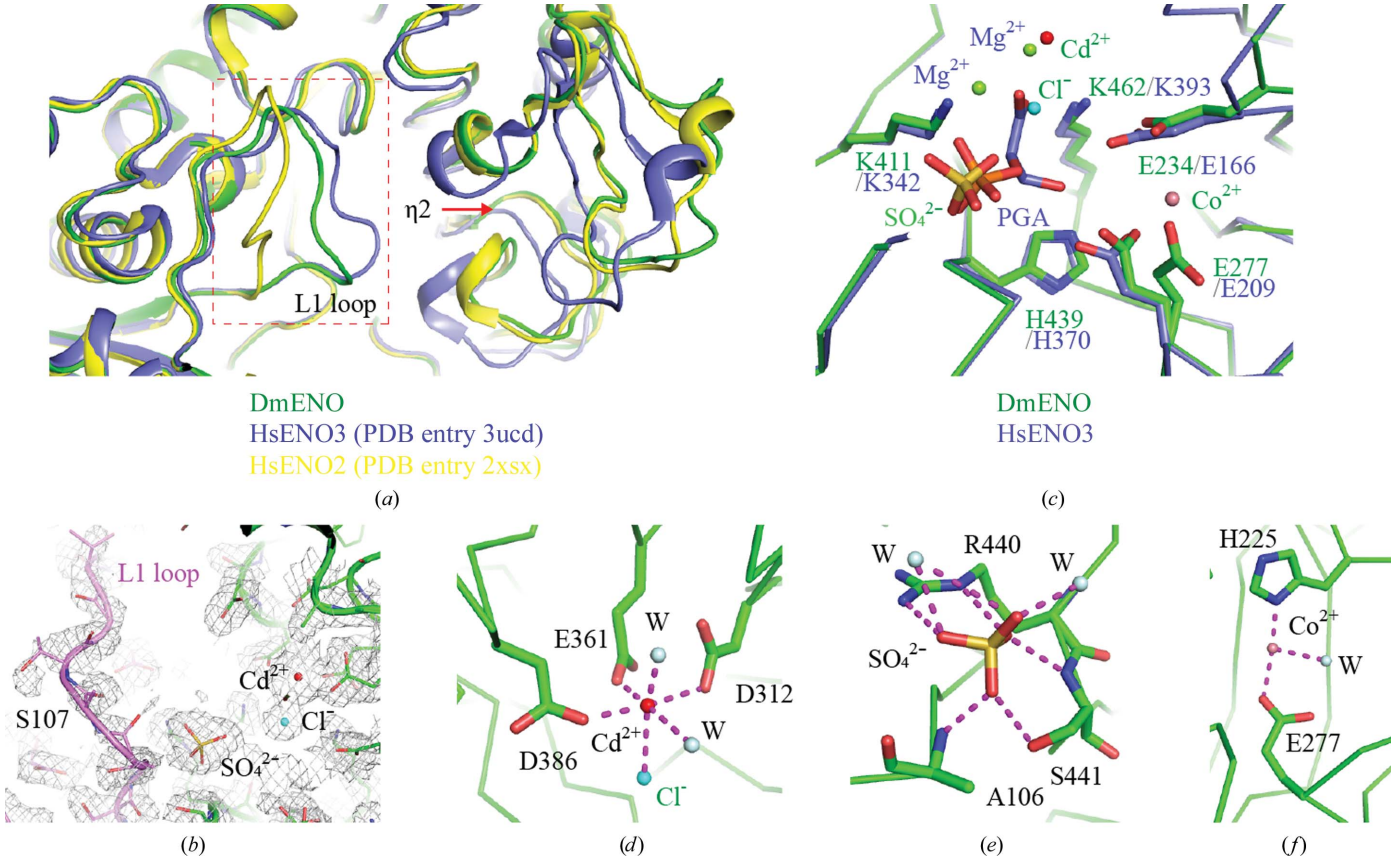

(*a*) (*c*) (*b*) (*d*) (*e*) (*f*)

Figure 3
(*a*) Structural comparison of DmENO with HsENO2 and HsENO3. DmENO, HsENO2 and HsENO3 are coloured green, slate and yellow, respectively. The red box indicates the L1 loop region. The red arrow shows that the η2 helix is distant from the active site. (*b*) The $2mF_o - DF_c$ map (grey mesh) for the active site of DmENO contoured at 1.0σ. The L1 loop is coloured purple. (*c*) Structural comparison of the active sites of DmENO and HsENO3. HsENO3 possesses two magnesium ions and the substrate PGA in its active site, while DmENO has one cadmium ion, one cobalt ion, one chloride ion and one sulfate ion in the active site. Residues involved in substrate binding and catalysis in DmENO and HsENO3 are shown as sticks. (*d*) The geometry and coordinates of the cadmium ion in the active site of DmENO. (*e*) The residues and waters interacting with the sulfate ion in the active site of DmENO. (*f*) The coordination of the cobalt ion in the active site of DmENO. The magenta dashed lines represent salt bridges and hydrogen bonds.

bonds. The main chain of Ser81 in the $\beta1/\beta2$ turn from one molecule forms hydrogen bonds to the main chain of Arg468 in the $\alpha13$ helix from the other molecule. The main chains of Val274 in the $\eta1/\alpha7$ loop from two molecules also contribute two hydrogen bonds. Interestingly, Val274 and Arg468 from two DmENO chains pack with each other through hydrophobic interaction. In addition, Tyr79 in the $\beta1$ strand of one chain and Met249 in the $\alpha6$ helix, and Leu472 and Leu479 in the $\alpha13$ helix from the other chain form hydrophobic packing. Residues responsible for side-chain-mediated contacts in the interface are highly conserved among different species (Supplementary Fig. S1).

3.3. The active site of DmENO

In our structure, DmENO does not contain either a reaction substrate or a product. The $\beta3/\alpha1$ loop (also named the L1 loop) of unliganded DmENO, as well as the $\eta2$ helix, is distant from the active site (Fig. 3*a*). Poor electron density and high temperature factors (average of 73.2 Å^2 for residues 105–112 in the L1 loop *versus* 41.0 Å^2 for the whole subunit) suggest that the L1 loop is structurally flexible (Fig. 3*b*). In addition, Ser107, which is crucial for catalysis, is partially disordered in the DmENO structure. When the DmENO structure was superposed with that of unliganded HsENO3 (PDB entry 3ucd; Qin *et al.*, 2012) in an open state, the root-mean-square deviation (r.m.s.d.) for C^α atoms only between the two structures was 0.389 Å, whereas the r.m.s.d. was 0.551 Å when it was aligned with liganded HsENO2 (PDB entry 2xsx; M. Vollmar, E. Krysztofinska, A. Chaikuad, T. Krojer, R. Cocking, F. Von Delft, C. Bountra, C. H. Arrowsmith, J. Weigelt, A. Edwards, W. W. Yue & U. Oppermann, unpublished work) in a closed state. The overall conformation of DmENO also resembles that of unliganded HsENO3, indicating that unliganded DmENO is in an open state (Fig. 3*a*).

The active site of DmENO is occupied by one cadmium ion, one cobalt ion, one chloride ion and one sulfate ion that are possibly from the crystallization solution (Figs. 3*b* and 3*c*). The cadmium ion replaces the magnesium ion in native enolases such as HsENO3 (PDB entry 3ucd) to coordinate the side

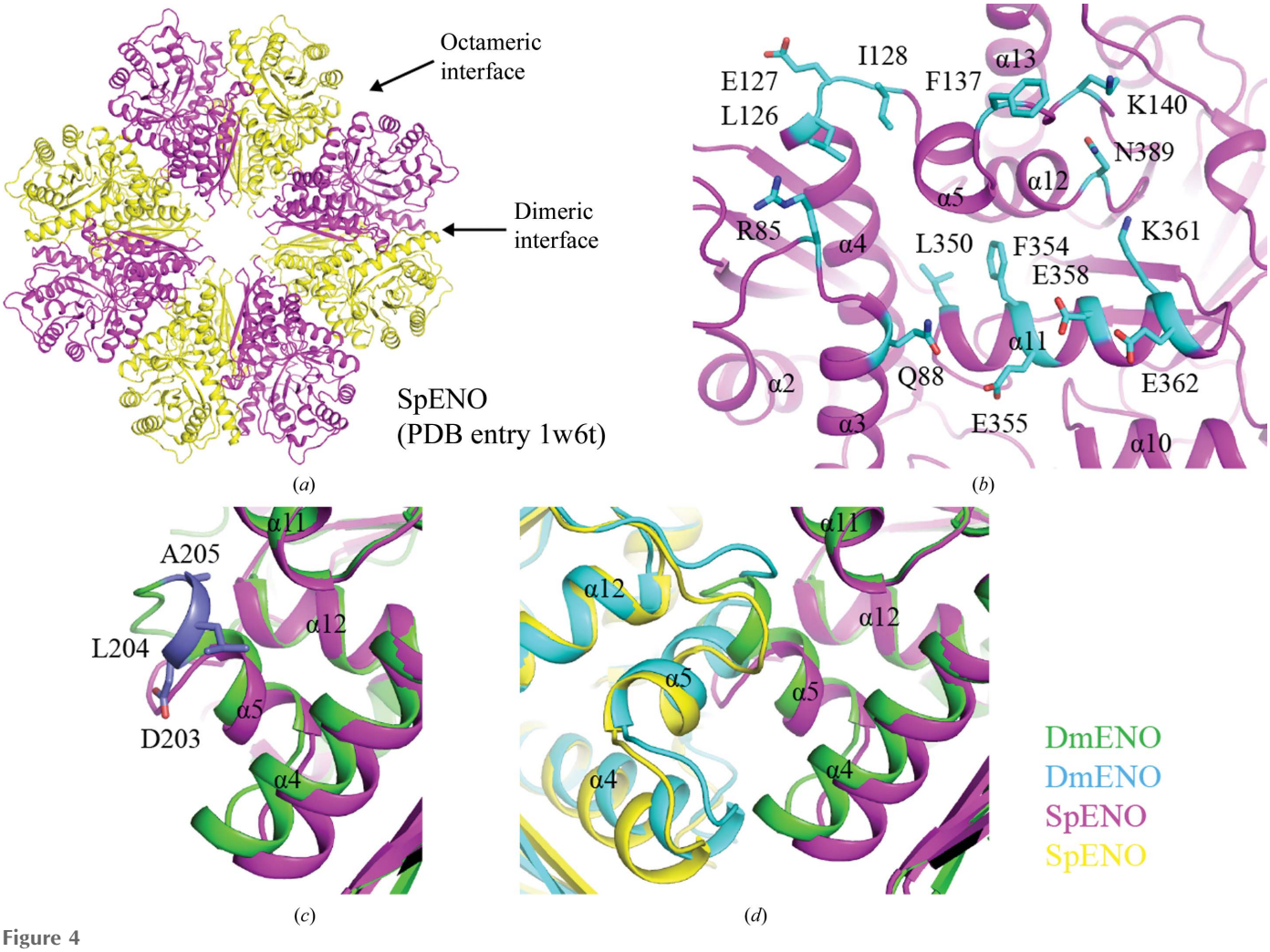

Figure 4
(*a*) Dimeric and octameric interfaces of SpENO. (*b*) Octameric interface of SpENO. Residues at the interface are coloured cyan and shown as sticks. Each secondary-structure element of SpENO is labelled according to those in DmENO. (*c*, *d*) Structural superposition of DmENO and SpENO. The two DmENO chains are coloured green and cyan, while the two SpENO chains are coloured magenta and yellow. The $\alpha5$ helix of DmENO is longer than that of SpENO. Residues in DmENO that are not present in SpENO are shown as slate sticks.

chains of Asp312, Glu361 and Asp386 of the enolase (Qin *et al.*, 2012; Figs. 3*c* and 3*d*). The cadmium ion also coordinates the chloride and two water molecules, forming an octahedral geometry just like the magnesium ion (Rulíšek & Vondrášek, 1998). The sulfate occupies the position of the phosphate moiety of the enolase substrate and forms salt-bridge and hydrogen-bond interactions with Ala106, Arg440 and Ser441 of DmENO (Figs. 3*c* and 3*e*). In HsENO3, Glu166, Glu209, Lys342, His370 and Lys393 contribute to the substrate-binding and catalytic activities (Qin *et al.*, 2012; Fig. 3*c*). When comparing the structure of DmENO with that of HsENO3, it was apparent that DmENO possessed the equivalent residues Glu234, Glu277, Lys411, His439 and Lys462. These residues have similar conformations, indicating that DmENO utilizes a similar catalytic mechanism to HsENO and thus has conserved function (Fig. 3*c* and Supplementary Fig. S1). The cobalt ion in the active site interacts with the side chains of His225 and Glu277 in DmENO (Figs. 3*c* and 3*f*). There is no metal ion present in the corresponding position of native enolases such as HsENO2 and HsENO3, suggesting that it is an artifact of crystallization.

3.4. Comparison of DmENO with octameric enolases

It has been reported that the enolases from some species, such as *S. pneumoniae* and *B. subtilis* enolase (SpENO and BsENO), exist as octamers (PDB entries 1w6t and 2pa6; Ehinger *et al.*, 2004; Newman *et al.*, 2012; Fig. 4*a*). The formation of the SpENO octameric interface involves many residues, including Arg85, Gln88, Leu126, Glu127, Ile128, Phe137, Lys140, Leu350, Phe354, Glu355, Glu358, Lys361, Glu362 and Asn389, which mediate extensive hydrogen-bonding, electrostatic and hydrophobic interactions (Ehinger *et al.*, 2004; Fig. 4*b*). When performing the sequence alignment of enolases from different species, we found that some crucial residues in the octameric interface are conserved in SpENO and BsENO, such as Leu126, Phe137, Lys140, Phe354, Glu355 and Asn389 in SpENO, but not in dimeric DmENO, HsENO1/2/3, ScENO1/2 and EcENO (Supplementary Fig. S1). Additionally, the α5 helix present in the octameric interface of SpENO, as well as BsENO, is shorter than that in DmENO (Fig. 4*c* and Supplementary Fig. S1). Three residues, Asp203, Leu204 and Ala205, in DmENO have no corresponding residues in SpENO and BsENO. When superposing the structures of DmENO and SpENO, we found that the longer α5 helix of DmENO clashes with the adjacent molecule, which precludes octamer formation (Fig. 4*d*). This longer α5 helix is also present in the human, yeast and *E. coli* enolases with a dimeric quaternary structure (Supplementary Fig. S1). Therefore, both specific amino acids and the α5 helix conformation determine that these dimeric enolases including DmENO do not form an octamer.

In this paper, we solved the crystal structure of DmENO. DmENO forms a homodimer just like the human and yeast enolases. In this structure, DmENO possesses an open conformation with a conformationally flexible L1 loop. This work provides a structural basis for further understanding of the functions of enolase in the fruit fly.

4. Related literature

The following references are cited in the Supporting Information for this article: Gouet *et al.* (1999) and Sievers *et al.* (2011).

Acknowledgements

We thank the staff of beamline BL17U at Shanghai Synchrotron Radiation Facility (SSRF) for help with data collection. We appreciate Dr Zhaocai Zhou for helpful support and discussion.

Funding information

Funding for this research was provided by: National Natural Science Foundation of China (award No. 81601442); Medical and Health Technology Development Program of Shandong Province (award No. 2016WS0524).

References

Adams, P. D. *et al.* (2010). *Acta Cryst.* D**66**, 213–221.
Afonine, P. V., Grosse-Kunstleve, R. W., Echols, N., Headd, J. J., Moriarty, N. W., Mustyakimov, M., Terwilliger, T. C., Urzhumtsev, A., Zwart, P. H. & Adams, P. D. (2012). *Acta Cryst.* D**68**, 352–367.
Battye, T. G. G., Kontogiannis, L., Johnson, O., Powell, H. R. & Leslie, A. G. W. (2011). *Acta Cryst.* D**67**, 271–281.
Buchan, D. W., Minneci, F., Nugent, T. C., Bryson, K. & Jones, D. T. (2013). *Nucleic Acids Res.* **41**, W349–W357.
Chai, G., Brewer, J. M., Lovelace, L. L., Aoki, T., Minor, W. & Lebioda, L. (2004). *J. Mol. Biol.* **341**, 1015–1021.
Díaz-Ramos, À., Roig-Borrellas, A., García-Melero, A. & López-Alemany, R. (2012). *J. Biomed. Biotechnol.* **2012**, 1–12.
Ehinger, S., Schubert, W. D., Bergmann, S., Hammerschmidt, S. & Heinz, D. W. (2004). *J. Mol. Biol.* **343**, 997–1005.
Emsley, P., Lohkamp, B., Scott, W. G. & Cowtan, K. (2010). *Acta Cryst.* D**66**, 486–501.
Feo, S., Arcuri, D., Piddini, E., Passantino, R. & Giallongo, A. (2000). *FEBS Lett.* **473**, 47–52.
Gerlt, J. A., Babbitt, P. C. & Rayment, I. (2005). *Arch. Biochem. Biophys.* **433**, 59–70.
Gouet, P., Courcelle, E., Stuart, D. I. & Métoz, F. (1999). *Bioinformatics*, **15**, 305–308.
Isgrò, M. A., Bottoni, P. & Scatena, R. (2015). *Adv. Exp. Med. Biol.* **867**, 125–143.
Kang, H. J., Jung, S.-K., Kim, S. J. & Chung, S. J. (2008). *Acta Cryst.* D**64**, 651–657.
Kühnel, K. & Luisi, B. F. (2001). *J. Mol. Biol.* **313**, 583–592.
López-Alemany, R., Longstaff, C., Hawley, S., Mirshahi, M., Fábregas, P., Jardí, M., Merton, E., Miles, L. A. & Félez, J. (2003). *Am. J. Hematol.* **72**, 234–242.
Lu, Q., Lu, H., Qi, J., Lu, G. & Gao, G. F. (2012). *Protein Cell*, **3**, 769–780.
McCoy, A. J., Grosse-Kunstleve, R. W., Adams, P. D., Winn, M. D., Storoni, L. C. & Read, R. J. (2007). *J. Appl. Cryst.* **40**, 658–674.
Murshudov, G. N., Skubák, P., Lebedev, A. A., Pannu, N. S., Steiner, R. A., Nicholls, R. A., Winn, M. D., Long, F. & Vagin, A. A. (2011). *Acta Cryst.* D**67**, 355–367.
Newman, J. A., Hewitt, L., Rodrigues, C., Solovyova, A. S., Harwood, C. R. & Lewis, R. J. (2012). *J. Mol. Biol.* **416**, 121–136.
Otwinowski, Z. & Minor, W. (1997). *Methods Enzymol.* **276**, 307–326.
Paludo, G. P., Lorenzatto, K. R., Bonatto, D. & Ferreira, H. B. (2015). *Comput. Biol. Chem.* **58**, 1–8.
Pancholi, V. (2001). *Cell. Mol. Life Sci.* **58**, 902–920.
Qin, J., Chai, G., Brewer, J. M., Lovelace, L. L. & Lebioda, L. (2012). *J. Inorg. Biochem.* **111**, 187–194.

Reed, G. H., Poyner, R. R., Larsen, T. M., Wedekind, J. E. & Rayment, I. (1996). *Curr. Opin. Struct. Biol.* **6**, 736–743.
Rulíšek, L. & Vondrášek, J. (1998). *J. Inorg. Biochem.* **71**, 115–127.
Sievers, F., Wilm, A., Dineen, D., Gibson, T. J., Karplus, K., Li, W., Lopez, R., McWilliam, H., Remmert, M., Söding, J., Thompson, J. D. & Higgins, D. G. (2011). *Mol. Syst. Biol.* **7**, 539.
Stec, B. & Lebioda, L. (1990). *J. Mol. Biol.* **211**, 235–248.
Subramanian, A. & Miller, D. M. (2000). *J. Biol. Chem.* **275**, 5958–5965.
Winn, M. D. *et al.* (2011). *Acta Cryst.* D**67**, 235–242.
Wu, Y., Wang, C., Lin, S., Wu, M., Han, L., Tian, C., Zhang, X. & Zang, J. (2015). *Acta Cryst.* D**71**, 2457–2470.